World Scientific
www.worldscientific.com

JAPAN SOCIETY OF CIVIL ENGINEERS
COASTAL ENGINEERING COMMITTEE

Coastal Engineering Journal, Vol. 59, No. 1 (2017) 1750006 (31 pages)

DOI: 10.1142/S0578563417500061

A Neural Network Tool for Predicting Wave Reflection, Overtopping and Transmission

Sara Mizar Formentin[*,‡], Barbara Zanuttigh[*,§]
and Jentsje W. van der Meer[†,¶]

[*]*University of Bologna, DICAM,*
Viale Risorgimento 2, 40136 Bologna, Italy

[†]*Van der Meer Consulting bv, P. O. Box 11,*
Akkrum, 8490 AA, The Netherlands

[†]*UNESCO IHE, Westvest 7,*
Delft, 2611 AX, The Netherlands

[†]*Delft University of Technology, Stevinweg 1,*
2628 CN, Delft, The Netherlands
[‡]*saramizar.formentin2@unibo.it*
[§]*barbara.zanuttigh@unibo.it*
[¶]*jm@vandermeerconsulting.nl*

Received 18 January 2016
Accepted 7 November 2016
Published 24 January 2017

This contribution presents a new Artificial Neural Network (ANN) tool that is able to predict the main parameters describing the wave-structure interaction processes: the mean wave overtopping discharge (q), the wave transmission and wave reflection coefficients (K_t and K_r). This ANN tool is trained on an extended database (based on the CLASH database) of physical model tests, including at least one of the three output parameters, for a total number of nearly 18,000 tests. The selected 15 nondimensional ANN input parameters represent the most significant effects of the structure type (geometry, amour size and roughness) and of the wave attack (wave steepness, breaking, shoaling, wave obliquity). The model can be used for design purposes, leading to a greater accuracy than existing formulae and similar tools for complex geometries for the prediction of K_r and K_t, and it has a similar accuracy as the CLASH ANN for predicting q.

Keywords: Artificial neural network; database; wave overtopping; wave reflection; wave transmission; breakwater.

[‡]Corresponding author.

1. Introduction

The assessment of the hydraulic performance of coastal and harbor structures for design purposes requires the accurate analysis of all the wave-structure interaction processes, such as wave overtopping, wave reflection and wave transmission. These phenomena are correlated to some extent, where dissipation of energy plays a role too. With respect to the wave energy balance, the higher the reflection, the lower the overtopping and the transmission. They can also be characterized by the same interacting factors, which are the physical parameters describing the wave attack and the structures features.

In the literature, several empirical formulae are available for the prediction of the key parameters representing the wave-structure interaction. Among others, it is worthy to mention EurOtop [2016] for the prediction of the wave overtopping discharge (q), Van der Meer *et al.* [2005] for the wave transmission coefficient (K_t) and Zanuttigh and van der Meer [2006, 2008] for the wave reflection coefficient (K_r). These analytical methods are targeted to represent specific structures types, often quite simple geometries and are far from providing a complete description of all coastal structures types and performances.

Different from the empirical formulae, the Neural Network modeling offers the possibility to include the effects of a large number of governing parameters, resulting in versatile tools able to represent complicated structure geometries and variable wave conditions. During the last years, successful examples of Artificial Neural Networks (ANNs) have been developed and used in Coastal Engineering in a wide range of applications [see the short review in Zanuttigh *et al.*, 2013]. The following works are limited to the ANNs representing (just) one of the processes involved in the wave-structure interaction: Van Gent *et al.* [2007] and Verhaeghe *et al.* [2008], for the prediction of q; Van Oosten and Peixò Marco [2005] and Panizzo and Briganti [2007], for K_t; Zanuttigh *et al.* [2013], for K_r.

Besides physical modeling, the contemporary representation of all the processes can be so far achieved only through advanced numerical modeling [e.g. Liu and Lin, 1997; Losada *et al.*, 2008], which often requires unaffordable computational efforts and also has its limits in numerical methods. On the contrary, an ANN model provides nearly instantaneous predictions and represents a great compromise between accuracy and time efficiency.

For the first time, Formentin and Zanuttigh [2013] and Zanuttigh *et al.* [2014] developed an unique ANN tool for the prediction of K_r and K_t and of K_r, K_t and q, respectively. Aim of the present contribution is to deliver an advanced ANN prediction tool for accurately and efficiently estimating q, K_r and K_t, by using consistently the same input parameters and ANN architecture. The strong conceptual motivation — and contemporary innovation — of the work is to prove that, as for the strict correlation among the physical processes, the traditionally fragmented approach based on finely tuned tools can be overcome by the delivery of just one tool adopting exactly the same parameters and structure.

This new ANN tool is intended to be delivered — upon registration only — to the Coastal Engineering community at www.unibo.it/overtopping-neuralnetwork, with the forthcoming publication of the updated EurOtop [2016].

The paper structure is as follows. Section 2 introduces the database used for training the ANN. The data, the setup and the structure parameters of CLASH [2004] were used as the starting point to gather and organize the other tests. Section 3 describes the general features of the ANN layout, examining both the input parameters and the fundamentals of the internal architecture, including the *bootstrap* resampling technique and the number of the hidden neurons. Section 4 illustrates the qualitative and quantitative performance of the new ANN tool with reference to all the output parameters, q, K_r and K_t. The predictions of the new ANN tool are compared with existing ANNs and literature formulae. The prediction of new datasets (i.e. datasets excluded from the training database) is provided as a validation of the ANN robustness. Conclusions and steps for further research are finally drawn in Sec. 5.

2. The Database

A homogenous database of 17,942 tests has been setup, by extending the database of 16,165 tests on wave reflection, transmission and overtopping already gathered by Zanuttigh *et al.* [2014]. This database in turn collected and re-organized the original CLASH database [Van der Meer *et al.*, 2009] on wave overtopping, the reflection database [Zanuttigh and van der Meer, 2008] and the DELOS database [Panizzo and Briganti, 2007] on wave transmission. Further details can be found in Zanuttigh *et al.* [2014]. The additional 1777 data consist of:

- 56 tests on rubble mound with cobs [Besley *et al.*, 1993];
- 20 tests on rubble mound with tetrapods [Goda *et al.*, 1975];
- 366 tests on smooth steep slopes by Victor and Troch [2012];
- 671 tests on smooth slopes in combination with walls by Van Doorslaer *et al.* [2015].
- 180 tests on vertical walls [of which, 117 from Goda *et al.*, 1975 and the remaining 63 from private communication];
- 75 tests on smooth structures with berms (private communication);
- 306 tests on reshaping berm breakwaters [of which 30 from Lykke Andersen *et al.*, 2008 and the remaining 276 from private communication];
- 103 tests on harbor caissons (private communication).

The schematization of the structures (see Fig. 1), the geometrical and the relevant climate parameters follow the structure already identified within the CLASH project and adopted by Zanuttigh *et al.* [2014]. Some modifications were introduced with respect to the CLASH database, such as the inclusion of new parameters and the setup of new calculation procedures.

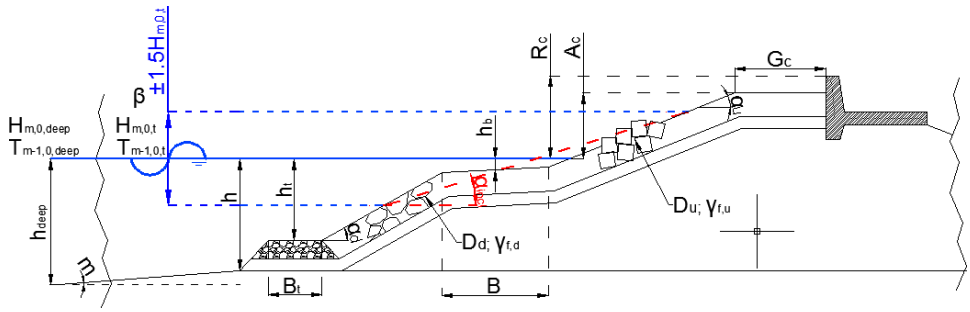

Fig. 1. Schematization of the structure based on CLASH, including some of the geometrical and hydraulic parameters.

One of the new parameters is the diameter D, representing the mean size of the structure elements in the run-up/down area. The D could be the $D_{n,50}$ for rock armor, D_n for concrete armor, but it could also be the height of a step of a staircase geometry. In principle it indicates the "size" of the structural elements, mainly around the water level. A smooth slope will get $D = 0$. The value of D is computed as the weighted average of the characteristic downslope D_d and upslope D_u sizes of the elements in the run-up/down area, i.e. within $\pm 1.5\, H_{m0,t}$ above and below the still water level, following the formula:

$$D = \frac{D_d \cdot (h_{\text{sub}} - h_b) + D_u \cdot (h_b + h_{em})}{h_{\text{sub}} + h_{em}}, \tag{1}$$

where $h_{\text{sub}} = \min(1.5 \cdot H_{m0,t}; h); h_{em} = \min(1.5 \cdot H_{m0,t}; A_c)$.

Consistent to the definition of Eq. (1), also the roughness factor γ_f and the average slope $\cot \alpha_{\text{incl}}$ (that is the average slope in the run-up/down area) are now respectively evaluated as

$$\gamma_f = \frac{\gamma_{fd} \cdot (h_{\text{sub}} - h_b) + \gamma_{fu} \cdot (h_b + h_{em})}{h_{\text{sub}} + h_{em}}, \tag{2}$$

$$\cot \alpha_{\text{incl}} = \frac{\cot \alpha_d \cdot (h_{\text{sub}} - h_b) + B + \cot \alpha_u \cdot (h_b + h_{em})}{h_{\text{sub}} + h_{em}}, \tag{3}$$

where the new parameters γ_{fd} and γ_{fu} are the roughness factors of the downslope and the upslope, attributed based on EurOtop [2016] and Bruce *et al.* [2006]. Equation (3) is valid for $|h_b| < 1.5 \cdot H_{m,0t}$; otherwise $\cot \alpha_{\text{incl}} = \cot \alpha_d (h_b > 0)$ *or* $\cot \alpha_{\text{incl}} = \cot \alpha_u (h_b < 0)$. The parameters appearing in the equations are all defined in Table 1.

A new label was introduced in the database, in order to identify tests with peculiar features, such as w = wind, p = prototype, c = current, b = bull nose, pc = perforated caisson. These tests were often given in CLASH a reliability factor RF = 4 to keep them outside from the ANN training, while in reality they could be quite reliable. RF indicates how reliable a test is on the basis of the available

Table 1. Parameters included in the new extended database compared with the ones included in the original CLASH database.

#	Parameter	Unit	Type	CLASH	New	Definition of the parameter
1	Name	[—]	general	√	√	
2	$H_{\mathrm{m0,deep}}$	[m]	hydraulic	√	√	Off-shore significant wave-height
3	$T_{p,\mathrm{deep}}$	[s]	hydraulic	√	√	Off-shore peak wave period
4	$T_{m,\mathrm{deep}}$	[s]	hydraulic	√	√	Off-shore average wave period
5	$T_{m-1,\mathrm{deep}}$	[s]	hydraulic	√	√	Off-shore spectral wave period
6	h_{deep}	[m]	structural	√	√	Off-shore water depth
7	m	[—]	structural	√	√	Foreshore slope
8	β	[°]	hydraulic	√	√	Wave obliquity
9	Spreading	[—]	hydraulic		√	Spreading
10	h	[m]	structural	√	√	Water depth at the structure toe
11	$H_{m0,t}$	[m]	hydraulic	√	√	Significant wave-height at the structure toe
12	$T_{p,t}$	[s]	hydraulic	√	√	Peak wave period at the structure toe
13	$T_{m,t}$	[s]	hydraulic	√	√	Average wave period at the structure toe
14	$T_{m-1,t}$	[s]	hydraulic	√	√	Spectral wave period at the structure toe
15	h_t	[m]	structural	√	√	Toe submergence
16	B_t	[m]	structural	√	√	Toe width
17	Type	[—]	structural	√	√	Type of structure and armor unit
18	$\cot\alpha_d$	[—]	structural	√	√	Cotangent of the angle that the
19	$\cot\alpha_u$	[—]	structural	√	√	part of the structure below/above the berm makes with a horizontal
20	$\cot\alpha_{\mathrm{excl}}$	[—]	structural	√	√	Cotangent of the mean angle that
21	$\cot\alpha_{\mathrm{incl}}$	[—]	structural	√	√	the structure makes with a horizontal, excluding/including the berm, in the run-up/ run-down zone
22	γ_{fd}	[—]	structural		√	Roughness factor for $\cot\alpha_d$
23	γ_{fu}	[—]	structural		√	Roughness factor for $\cot\alpha_u$
24	γ_f	[—]	structural	√	√	Roughness factor [average in the run-up/down area in the new DB, Eq. (2)]
25	D_d	[—]	structural		√	Size of the structure elements along $\cot\alpha_d$
26	D_u	[—]	structural		√	Size of the structure elements along $\cot\alpha_u$
27	D	[m]	structural		√	Average size of the structure elements in the run-up/down area [Eq. (3)]
28	R_c	[m]	structural	√	√	Crest height with respect to swl
29	B	[m]	structural	√	√	Berm width
30	h_b	[m]	structural	√	√	Berm submergence
31	$\tan\alpha_b$	[—]	structural	√	√	Berm slope
32	B_h	[m]	structural	√	√	Horizontal berm width

Table 1. (*Continued*)

#	Parameter	Unit	Type	CLASH	New	Definition of the parameter
33	A_c	[m]	structural	√	√	Wall height with respect to swl
34	G_c	[m]	structural	√	√	Crest width
35	RF	[—]	general	√	√	RF
36	CF	[—]	general	√	√	CF
37	Pow	[—]	hydraulic	√	√	Overtopping probability
38	q	[m^3/s/m]	hydraulic	√	√	Average specific wave overtopping discharge
39	K_r	[—]	hydraulic		√	(Bulk) Wave reflection coefficient
40	K_t	[—]	hydraulic		√	(Bulk) Wave transmission coefficient
41	Core data	[—]	general		√	Flag indicating the inclusion/exclusion from the "core" data of the ANN training

information (which parameters on wave conditions and foreshore geometry were available and which estimations had to be made because of missing parameters), the restrictions/possibilities of the test facility used to perform the test and the precision of the measurements and analysis of the researcher who performed the test [Verhaeghe, 2005]. CF indicates how well a structure geometry could be described by the geometrical parameters considered in the database. A value of 4 means that the test was so unreliable or so complex that it should not be considered neither for further analysis nor for training. The new label (an extra column in the database) allows to separate all the "peculiar" tests from the "core" data, i.e. to the data selected for the training database, without attributing them an artificial RF = 4. Following CLASH, the definition of the reliability factor (RF) and complexity factor (CF) is still adopted to exclude from training the core-data that are actually given either RF = 4 or CF = 4.

In conclusion, the final "extended" database counts 8 parameters more than the CLASH database and now consists of:

- 14 hydraulic parameters, of which 11 characterizing the wave attack conditions (extension with the spreading parameter, as all the reports include this value in the case of short-crested waves; long-crested waves have the *spreading* = 0) and 3 representing the "output" parameters (q, K_r and K_t);
- 23 structural parameters (extension with D, D_d, D_u, γ_{fd} and γ_{fu});
- 4 general parameters, the test name/label, the reliability RF and the complexity CF factors, and a flag indicating the inclusion/exclusion from the "core" data for the ANN training;

Table 1 reports the type and the number of all the parameters included in the extended database, in comparison with the original CLASH database.

Following the division proposed by Zanuttigh and van der Meer [2008], the extended database is categorized into 7 sections [Zanuttigh *et al.*, 2014], labeled progressively from A to G, in order to distinguish different types of structures and/or wave attack conditions. These categories are: straight permeable rock slopes ("A"), straight impermeable rock slopes ("B"), armor units with straight slopes ("C"), smooth and straight slopes ("D"), structures with combined slopes and berms ("E"), vertical walls ("F") and oblique wave attack ("G").

With respect to availability of data at present the following conclusions can be drawn.

- For q, a total amount of 13,511 tests are available, of which 1733 are non-core data, 1128 are given either RF or CF = 4 and further 2456 tests were discarded because, following Van Gent *et al.* [2007], only the tests with $q \geq 10^{-6}\,\mathrm{m}^3/\mathrm{s/m}$ were considered. The ANN was therefore trained on the remaining 8194 tests (61%).
- For K_r, 7371 tests are available, of which 1066 are noncore data and 527 tests are given either RF or CF = 4; therefore, the training database is composed by 5778 (78%) tests.
- For K_t, a total amount of 3587 tests is available, of which 3275 (91%) are used for the ANN training, being 34 the noncore data and 278 the tests with RF or CF = 4.

Table 2. Overview of the database divided into the 3 main datasets used to train the ANN. For each dataset, the indication of the range of the key parameters (i.e. the input parameters of the ANN, see Subsec. 3.3) is given.

	Reflection dataset		Overtopping dataset		Transmission dataset	
	min	max	min	max	min	max
Input Parameter						
$H_{m0,t}/L_{m-1,0,t}$	3.05e−04	0.086	0.001	0.085	0.001	0.077
β	0.000	83.490	0.000	80.000	0.000	68.550
$h/L_{m-1,0,t}$	0.000	0.829	0.003	0.942	0.003	0.467
$h_t/H_{m0,t}$	0.375	29.167	0.430	23.333	0.732	38.462
$B_t/L_{m-1,0,t}$	0.000	0.264	0.000	0.760	0.000	0.336
$h_b/H_{m0,t}$	−2.133	7.833	−1.347	7.833	−1.702	6.093
$B/L_{m-1,0,t}$	0.000	0.684	0.000	0.972	0.000	0.289
$A_c/H_{m0,t}$	−8.086	12.051	−5.247	16.076	−10.000	9.615
$R_c/H_{m0,t}$	−8.086	12.051	0.000	16.076	−10.000	9.615
$G_c/L_{m-1,0,t}$	0.000	2.003	0.000	0.362	0.000	2.003
m	0.000	1000.0	0.000	1000.0	0.000	1000.0
$\cot\alpha_d$	0.000	7.000	0.000	7.000	0.000	5.000
$\cot\alpha_{\mathrm{incl}}$	−0.491	10.638	−1.179	11.299	0.000	6.836
γ_f	0.340	1.000	0.330	1.000	0.380	1.000
$D/H_{m0,t}$	0.000	6.539	0.000	2.000	0.000	10.385
Scale Parameter						
$H_{m0,t}$ [m]	0.005	1.850	0.017	1.480	0.005	1.355
$L_{m-1,0,t}$ [m]	0.575	117.904	0.691	156.944	0.575	54.515

The range of the key parameters for each dataset is reported in Table 2. The three main datasets are only partially overlapping, giving significantly smaller sub-datasets with more than 1 of the outputs parameters.

3. The New Artificial Neural Network Tool

3.1. *General features of an ANN model*

An ANN is essentially a regression model which reconstructs the input-output functional relationships underlying a physical process. During the calibration, the model "learns" the input–output relationships from a set of experimental data, and provides the fitting function $\bar{y} = f(\bar{X})$ which best reproduces the links among the *input parameters* ($\bar{X}$) and the corresponding *output parameters* ($\bar{y}$). Generally, an ANN includes at least one *hidden layer* containing an arbitrary number of *hidden neurons*, which do not represent any physical quantity and are used only to increase the degrees of freedom of the ANN. The numerical information contained in the input parameters is elaborated by the ANN and passed to the first (or unique) hidden layer through the so-called *hidden layer transfer function*. Similarly, the following hidden layers — if existing — receive the information from the previous hidden layer through other transfer functions, up to the output/s. Each input parameter is connected to each hidden neuron, and the hidden neurons are likewise connected to the output layer, which can consist of one or more output parameters. The ensemble of neurons, layers and connections of an ANN defines its *architecture* and determines its characterizing fitting function $\bar{y} = f(\bar{X})$.

The process of training the ANN essentially consists of the definition of the numerical weights to be assigned to each connection. This process, governed by the training algorithm, is based on the iterative research of the minimum error among the outputs predicted by the ANN itself and the experimental target values. The velocity and the efficiency of the training depend on the transfer functions, the error type to minimize and the tolerance imposed and on the training algorithm. Once the ANN is trained, or calibrated, it can be used to provide predictions of new data. A standard pc will get nearly instantaneous predictions for thousands of tests, comparable to a spreadsheet.

3.2. *The basic ANN architecture*

The new tool we are going to propose here is composed of three similar ANN models (i.e. three similar but independent fitting tools) characterized by the same architecture. Each ANN model is trained on 1 of the 3 separate datasets including K_r or K_t or q.

The starting ANN architecture is directly derived from the works recently carried out by the authors [Zanuttigh *et al.*, 2013, 2014]. The effects of adopting different training algorithms, combinations of input parameters, techniques to improve the

ANN capability of generalization were analyzed in depth and led to a final set of optimal ANN characteristics. Two modifications of such optimized scheme are introduced here, and specifically consist of: the final selection of the input parameters (in Sec. 3.3) and the revision of the number of hidden neurons (in Sec. 3.5).

The resulting features of the ANN architecture, built in the MATLAB environment, are resumed in the following:

- 15 dimensionless input parameters (described in Sec. 3.3);
- multilayer network, based on a *feed-forward back-propagation* learning algorithm, 1 hidden layer, and 1 output layer:
  - — the hidden layer consists of 20 hidden neurons, see the sensitivity analysis in Sec. 3.5;
  - — the output layer consists of 1 output parameter (i.e. K_r or $K_t$or q);
- training algorithm: *Levenberg–Marquardt* [Marquardt, 1963; Hagan and Menhaj, 1994]. It is proved in Zanuttigh *et al.* [2013] that this algorithm ensures the best compromise between ANN performance and computing efficiency;
- hidden neurons transfer function: *hyperbolic tangent sigmoid function*, which corresponds to the expression $f_1(n) = \frac{2}{1+\exp(-2n)} - 1$, where n is a generic variable that can assume every value from $-\infty$ to $+\infty$. Such tan-sigmoid transfer function accomplishes the two paramount requisites of continuity and nonlinearity (the relationship between the output quantities K_r, $K_t q$ and the input parameters are hardly nonlinear) and allows negative outputs (matching the logarithmic transformed values of q).
- output neuron transfer function: *linear transfer function*, $f_2(n) = n$; therefore, the resulting fitting function represented by the ANN model and resulting from the composition of f_1 and f_2 is provided by:

$$y = \mathrm{LW} \cdot \left(\frac{2}{(1 + \exp(-2 \cdot (\mathrm{IW} \cdot \bar{X} + b_1)))} - 1 \right) + b_2, \tag{4}$$

  where $\bar{X}$ represents the input parameters array (sized $[15 \times 1]$), y is the scalar output of the model, IW is the *Input Weights* matrix (sized $[20 \times 15]$, connecting the 20 hidden neurons to the 15 input parameters $\bar{X}$), LW is the *Layer Weights* matrix (sized $[1 \times 20]$, connecting the single output neuron to the 20 hidden neurons), b_1 is the *bias array* of the *hidden layer* ($[20 \times 1]$, connecting the 20 hidden neurons to the bias) and b_2 is the scalar *bias* of the *output layer* (it connects the single output parameter to the bias of the output layer).
- error type: Mean Squared Error (MSE);
- maximum number of iterations allowed: 100;
- method to improve generalization: none. The assessment of the ANN performance is attributed to the *bootstrap resampling* technique (see Zanuttigh *et al.* [2014] and Sec. 3.4);

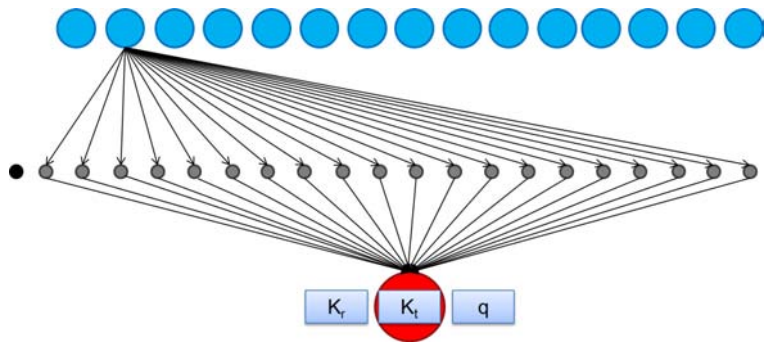

Fig. 2. Schematization of the conceptual layout of an ANN. In the new ANN, the input layer consists of 15 input parameters, the hidden layer of 20 hidden neurons and 1 bias, and the output layer consists of 1 output neuron that can be q, K_r or K_t.

- the results are derived from the commitment of more ANNs and are provided as quantiles of the statistical distribution of all the ANNs results (see Secs. 3.4 and 3.6).

The conceptual schematization of the ANN architecture is provided in Fig. 2.

The number of tests required to "properly" train the ANN strictly depends on the number of input parameters, hidden neurons and output parameters, i.e. by the overall number of freedom degrees N_{fd} characterizing the ANN. This number is given by the following expression

$$N_{\text{fd}} = N_{\text{hn}} \cdot N_X + N_y \cdot N_{\text{hn}} + N_{b_1} \cdot N_{\text{hn}} + N_y \cdot N_{b_2}, \tag{5}$$

where: N_{hn} = number of hidden neurons (20); N_X = number of input parameters (15); N_y = number of output parameter/s(1); $N_{b_1} = N_{b_2}$ = number of biases (1 per layer). Therefore, N_{fd} is equal to 341 (see Table 2).

N_{fd} essentially is the number of calibration parameters, i.e. the weights IW, LW and the biases b_1, b_2 as defined in Sec. 3.1. The value of N_{fd} becomes important when the amount of available tests is modest and a reduction of N_{fd} is pursued (see Sec. 3.5) or when it is used as element of comparison between 2 ANNs (see Sec. 4.2). The accurate assessment of IW and LW is dependent not only on the number, but also on the sorting of the tests, i.e. on the variety of represented geometries and wave conditions.

3.3. *The ANN input parameters*

Based on the previous work carried out by the authors [Zanuttigh *et al.*, 2014], the input parameters are made dimensionless with physically based motivations. The way the parameters are made dimensionless differs from the ANN by Van Gent *et al.* [2007], where the parameters are re-scaled according to the Froude Law based on the same prototype condition, by using the "scaling factor" $H_{m0,t} = 1\,\text{m}$. The full list of dimensionless input parameters is given in Table 3.

Table 3. Synthesis of the 15 selected dimensionless input parameters and 3 output parameters of the new ANN tool.

#	Input Parameter	Type	Representation of
1	$H_{m0,t}/L_{m-1,0,t}$	Wave attack	Wave steepness
2	β	Wave attack	Wave obliquity
3	$h/L_{m-1,0,t}$	Wave attack	Shoaling parameter
4	$h_t/H_{m-1,0,t}$	Geometry	Effect of the toe submergence
5	$B_t/L_{m-1,0,t}$	Geometry	Effect of the toe width
6	$h_b/H_{m0,t}$	Geometry	Effect of the berm submergence
7	$B/L_{m-1,0,t}$	Geometry	Effect of the berm width
8	$A_c/H_{m0,t}$	Geometry	Effect of crest submergence
9	$R_c/H_{m0,t}$	Geometry	Effect of crest submergence in presence of a crown wall
10	$G_c/L_{m-1,0,t}$	Geometry	Effect of the crest width
11	m	Geometry	Effects of the foreshore slope
12	$\cot\alpha_d$	Geometry	Down slope
13	$\cot\alpha_{\text{incl}}$	Geometry	Average slope in the run-up/down area
14	$D/H_{m0,t}$	Structure characteristics	Indication of structure permeability
15	γ_f	Structure characteristics	Dissipation induced by structure roughness
	Output parameter		Representation of
	K_r		Wave reflection coefficient
	K_r		Wave reflection coefficient
	$q^* = \frac{\log_{10}(q_{AD})-\min\{\log_{10}(q_{AD})\}}{\lvert\min\{\log_{10}(q_{AD})\}-\max\{\log_{10}(q_{AD})\}\rvert}$, $q_{AD} = \frac{q}{\sqrt{gH^3_{m,0,t}}}$		Wave overtopping discharge

The parameters related to the wave attack represent wave breaking due to wave steepness and water depth, shoaling and effects induced by wave obliquity. The parameters describing structure heights (vertical measures of toe, berm, crest) are all made dimensionless with the significant wave-height, to represent the effects induced by local breaking and by wave run-up. The parameters describing structure widths (horizontal measures of toe, berm, crest) are all made dimensionless with the wave length, to account for the induced local reflection that might be in phase or not with the wave reflection from other parts of the structure slope. Characteristic structure slopes include the down slope, as it is the most important one in the wave reflection process, and the average slope in the run-up/down area, as it proved to be the most relevant for estimating wave overtopping in case of complex structures.

3.4. *The* bootstrap *resampling technique in the training process*

As stated in Sec. 3.2, the predictions of the output parameters are derived from the commitment of several ANNs. This process, i.e. the commitment, is carried

out to perform a statistical analysis of the ANN results and therefore derive more representative output values.

The application of the *bootstrap* technique consists of training the ANN on several (N) *bootstrapped* databases, which have the same size as the original database but include a different assortment of data. In each of the N *bootstrapped* databases the tests are selected from the original database with replacement, i.e. the same test may appear once, more than once or never and in this latter case it is replaced by another test that necessarily appears then at least twice.

Following the previous work by Van Gent *et al.* [2007] and Verhaeghe *et al.* [2008], the selection of the data is here driven by the Weight Factors WF:

$$\mathrm{WF} = (4 - \mathrm{RF}) \cdot (4 - \mathrm{CF}), \tag{6}$$

where RF and CF are respectively the reliability and CFs, as defined in Sec. 2 and in Table 1.

The higher the WF (that may range between 0 and 9, according to the values of RF and CF that vary between 1 and 4) the higher the probability for a test to be selected. This means that more weight was given to reliable and noncomplex tests. The distribution and the sorting of the WF values within the three databases of wave overtopping, transmission and reflection are reported in Fig. 3, through the use of frequency histograms. For each database, the percentages refer to the overall amount of tests (i.e. 13,511, 7371 and 3587, for q, K_r and K_t respectively, see Sec. 2), including the noncore data and all the values of q.

Figure 3 shows that nearly 10% of the wave overtopping and reflection tests belongs to the "class" 0 (i.e. WF = 0), which means that it is discarded from the

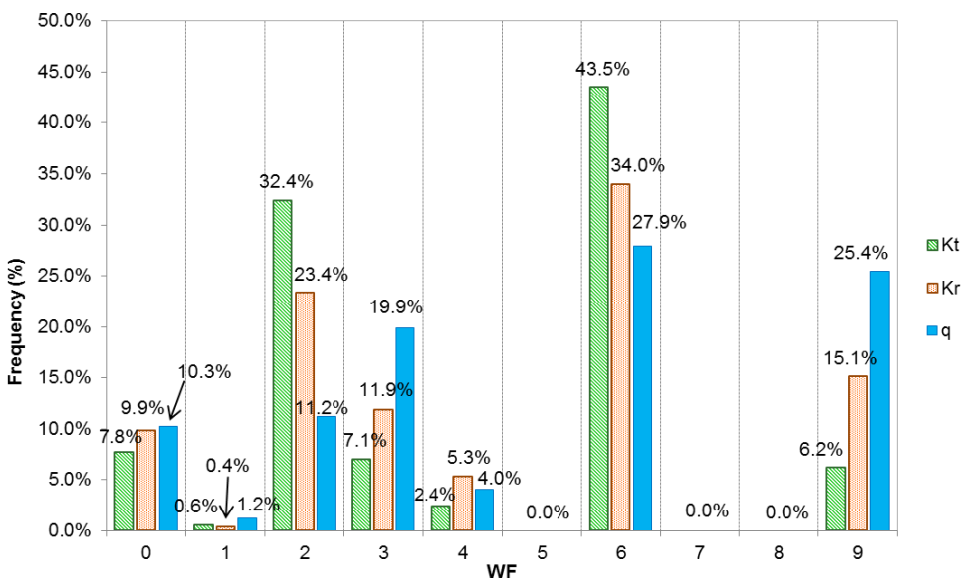

Fig. 3. Distribution and percentages of the values of the WF for the 3 databases.

training (see Sec. 2). This percentage is slightly lower ($\approx 8\%$) for the transmission database. The two higher classes of WF (i.e. 6 and 9) include approximately half of the data of q, K_r and K_t, while the 4 remaining lower classes of WF (1–4) altogether represent only 35–40% of the databases. From Fig. 3 it is evident that the WF for K_t and K_r are not equally distributed and that a great predominance of values in the classes 2 and 6 is detected, while the values of q are similarly distributed throughout the classes 3, 6 and 9. The effect of weighting a group of tests much higher than another group systematically forces the ANN training toward that given set of data. These are the ones considered to be more reliable and whose structure was better represented by the schematization in Fig. 1.

The *bootstrap* resampling of the database is adopted here to assess the performance of the ANN. Each differently trained ANN gives different estimates of the output parameter, and the ensemble of the predicted outputs can be considered as a stochastic variable and therefore used to derive average indexes of performance and standard deviations. Furthermore, if the number of resamples is large-enough to be statistically significant, it is possible to calculate the quantiles of the distribution and derive the confidence intervals [Van Gent *et al.*, 2007]. The mean prediction is not only more significant from a statistical view-point, but it is also more accurate than the prediction of a single ANN, as it adopts the output of several trained ANNs (see further details in Sec. 3.6).

The mean predictions ($\langle y \rangle$) of each output parameter are computed through an average process of the M single predictions (y, see Eq. (4)) obtained from the M *bootstrapped* ANNs:

$$\langle y \rangle = \frac{1}{M} \sum_{i=1}^{M} \mathrm{LW}_i \cdot \left(\frac{2}{(1 + \exp(-2 \cdot (\mathrm{IW}_i \cdot \bar{X} + b_{1i})))} - 1 \right) + b_{2i}, \tag{7}$$

where the subscript i indicates the ith *bootstrapped* ANN characterized by the ith weights matrices IW_i and LW_i and biases b_{1i} and b_{2i}. A similar average process [see Eq. (14)] is applied to all the error indexes of Eqs. (8)–(10) and (13), see Sec. 3.6.

All the average values and corresponding standard deviations of Tables 4 and 8 and of Fig. 4, and the 95% confidence bands in the figures characterizing the performance of the ANN (Figs. 5–10) are drawn on the basis of the statistical distribution derived from the bootstrapping and the commitment.

3.5. *The number of hidden neurons and the ANN architecture "complexity"*

The definition of the number of hidden neurons (N_{hn}) — which represents one of the key features of an ANN — is generally related to the number of input parameters (N_X) and to the range of variability of the input data, but it cannot be defined *a priori*. Together with N_X, N_{hn} contributes to determine the number of the ANN degrees

Table 4. Synthesis of the performance of the ANN obtained with the adoption of the *bootstrapping* technique and the "commitment of networks" [as in Van Gent *et al.*, 2007]. The values of the indexes are averaged from 500 *bootstrap* resamplings of the database. For the prediction of the overtopping, the index RMSE is computed to the transformed values of q (see Sec. 3.6).

	RMSE and RMSE*	WI	R^2	Large errors (%)
Overtopping discharge, $q \geq 10^{-6}$ m^3/s/m (# 8,194)	0.052 ± 0.005	0.974 ± 0.006	0.90 ± 0.02	7.0
Wave reflection coefficient, K_r (# 5,778)	0.035 ± 0.004	0.990 ± 0.003	0.96 ± 0.01	5.5
Wave transmission coefficient, K_t (# 3,275)	0.034 ± 0.008	0.995 ± 0.004	0.99 ± 0.02	10.0

Table 5. Input parameters and required training data of the three existing ANN selected for comparison with the new ANN tool here presented.

	K_r [Zanuttigh *et al.*, 2013]	K_t [Panizzo and Briganti, 2007]	q [Van Gent *et al.*, 2007]	New ANN tool
Input Parameters				
1	$H_{m0,t}/L_{m-1,0,t}$	$R_c/H_{m0,t}$	$H_{m0,t}$	$H_{m0,t}/L_{m-1,0,t}$
2	$h_t/L_{m-1,0,t}$	$G_c/L_{m-1,0,t}$	$T_{m-1,t}$	β
3	γ_f	$G_c/H_{m0,t}$	γ_f	$h/L_{m-1,0,t}$
4	$\cot\alpha_d$	$H_{m0,t}/h$	$\cot\alpha_d$	$h_t/H_{m-1,0,t}$
5	$\cot\alpha_{\text{incl}}$	$\xi_{0,p}$	$\cot\alpha_u$	$B_t/L_{m-1,0,t}$
6	$D/H_{m0,t}$	$H_{m0,t}/D$	B	$h_b/H_{m0,t}$
7	$R_c/H_{m0,t}$		B_t	$B/L_{m-1,0,t}$
8	$B/L_{m-1,0,t}$		h	$A_c/H_{m0,t}$
9	$h_b/H_{m0,t}$		h_t	$R_c/H_{m0,t}$
10	$G_c/L_{m-1,0,t}$		h_b	$G_c/L_{m-1,0,t}$
11	m		R_c	m
12	β		A_c	$\cot\alpha_d$
13	*Spreading*		G_c	$\cot\alpha_{\text{incl}}$
14			$\tan\alpha_B$	$D/H_{m0,t}$
15			β	γ_f
Training				
N_x — Eq. (5)	13	7	15	15
N_{HN} — Eq. (5)	40	6	20	20
N_{fd} — Eq. (5)	601	55	341	341
# data	5,781	2,285	8,372	See Sec. 2

of freedom N_{fd} and consequently its versatility in recognizing the input–output relations. Generally, the higher N_{hn}, the better the ANN performance. However, a too high value of N_{hn} may induce overtraining problems and reduce, on the contrary, the ANN capability of generalization. Besides, the number of tests required for the ANN training increases significantly with N_{fd} and therefore with N_{hn}, see Sec. 3.2 and Eq. (5), where N_{hn} appears 3 times and is clearly the dominating element. The

Table 6. Summary of the performance of the existing ANNs for the 3 outputs: q [Van Gent *et al.*, 2007], K_r [Zanuttigh *et al.*, 2013], K_t [Panizzo and Briganti, 2007]. Van Gent *et al.* [2007] provided the error for $\log(q_{AD})$, which differs from the target q^* used for the new ANN tool, see Eqs. (11) and (13).

Performance of the existing ANNs				
Output	RMSE	WI	R^2	Large errors (%)
$\log q_{AD}$	0.29	—	—	—
K_r	0.038 ± 0.003	0.985 ± 0.003	0.943 ± 0.006	2.5%
K_t	0.065	—	0.983	—

Table 7. Comparison of the performance of the existing formulae for K_r [Zanuttigh and van der Meer, 2006, 2008], K_t [Van der Meer *et al.*, 2005] and q [EurOtop, 2016] and of the new ANN tool. Different datasets have been used according to the range of validity of the formulae.

Prediction of K_r												
Type of structure	Rock perm. (#337)			Rock imp. (#117)			Arm. Units (#416)			Smooth imp. (#349)		
(# nr. of tests)	RMSE	WI	R^2	RMSE	WI	R^2	RMSE	WI	R^2	RMSE	WI	R^2
Formula	0.066	0.852	—	0.068	0.918	0.70	0.052	0.888	0.51	0.113	0.947	0.83
ANN	0.032	0.967	0.86	0.037	0.976	0.90	0.031	0.964	0.85	0.030	0.995	0.98

Prediction of K_t						
	$G_c/H_{m,0,t} < 8$ (#2,128)			$G_c/H_{m,0,t} > 12$ (#530)		
Range (# nr. of tests)	RMSE	WI	R^2	RMSE	WI	R^2
Formula	0.108	0.912	0.71	0.084	0.95	0.82
ANN	0.032	0.990	0.96	0.031	0.992	0.97

Prediction of q			
	(#1,806)		
(# nr. of tests)	RMSE*	WI	R^2
Formula	0.075	0.937	0.75
ANN	0.045	0.977	0.92

assessment of the optimal number of hidden neurons must represent a good compromise among the "complexity" of the architecture and the performance obtained.

The common methodology [Van Gent *et al.*, 2007; Panizzo and Briganti, 2007] to establish the optimal value of N_{hn} consists of testing the ANN performance as a function of the progressive increase in the number of the N_{hn} themselves. In the present work, the analysis of the N_{hn} has been carried out for each output K_r, K_t and q and the optimal number has finally been defined as the most suitable for all the outputs.

Table 8. Quantitative performance of the new ANN tool when predicting K_r for datasets excluded from the training DB. The error index is not provided when the computed standard deviation is of the same order of magnitude of the average value of the index itself.

Dataset	Armor type (DB group)	RMSE [—]	WI [—]	R^2 [—]	Large errors [%]
Training dataset (#5,456)	All	0.035 ± 0.004	0.990 ± 0.003	0.96 ± 0.01	5.4
Kramer *et al.* [2005]	Rocks LCS (A)	0.052 ± 0.02	0.919 ± 0.06	0.77 ± 0.1	5.7
—	Tetrapods (C)	0.056 ± 0.08	0.705 ± 0.1	—	23
—	Smooth dikes (D)	0.046 ± 0.05	0.914 ± 0.08	0.54 ± 0.4	6.0
—	Smooth berms (E)	0.044 ± 0.06	0.902 ± 0.09	—	5.0
—	Reshaping b.b. (E)	0.038 ± 0.03	0.927 ± 0.1	0.77 ± 0.2	1.0

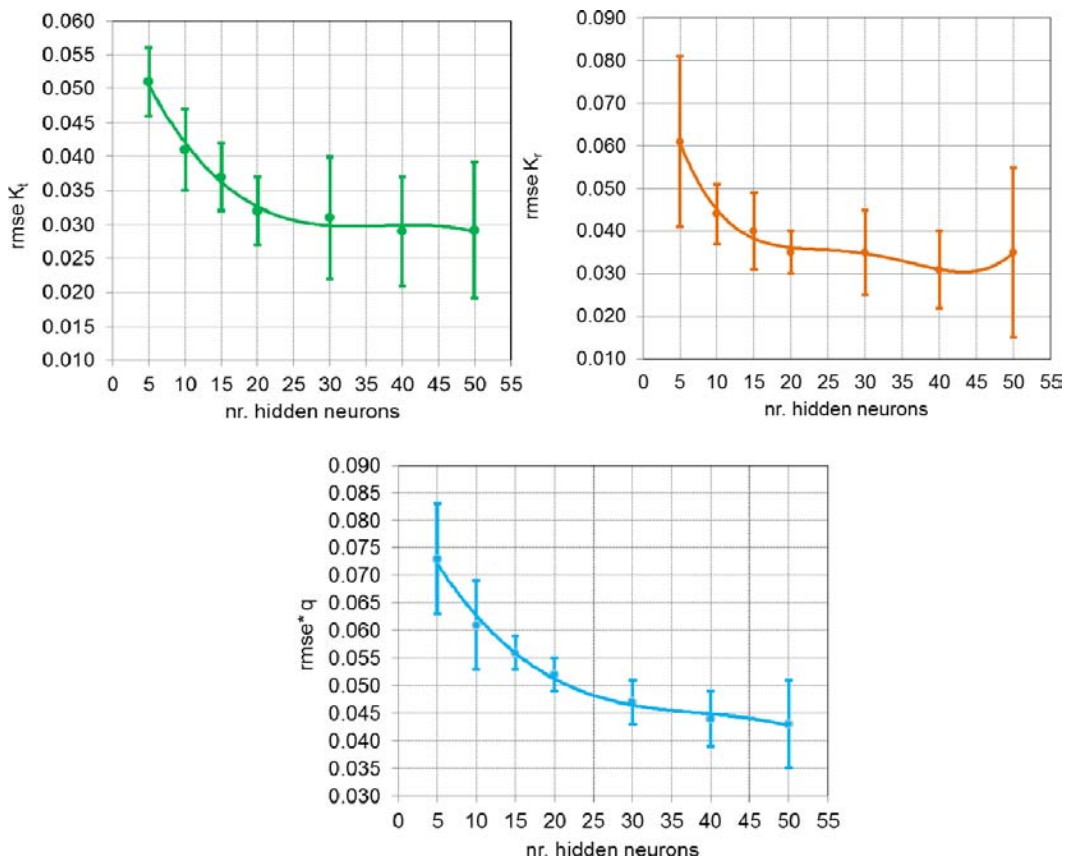

Fig. 4. Average values and corresponding standard deviations of the RMSE indexes derived after 500 *bootstrap* resamples of the ANN tool for a varying number of hidden neurons. From left to right and from top to bottom: wave transmission, reflection and overtopping. In case of overtopping, the index RMSE* computed from the transformed values of q, see Eq. (13), is shown.

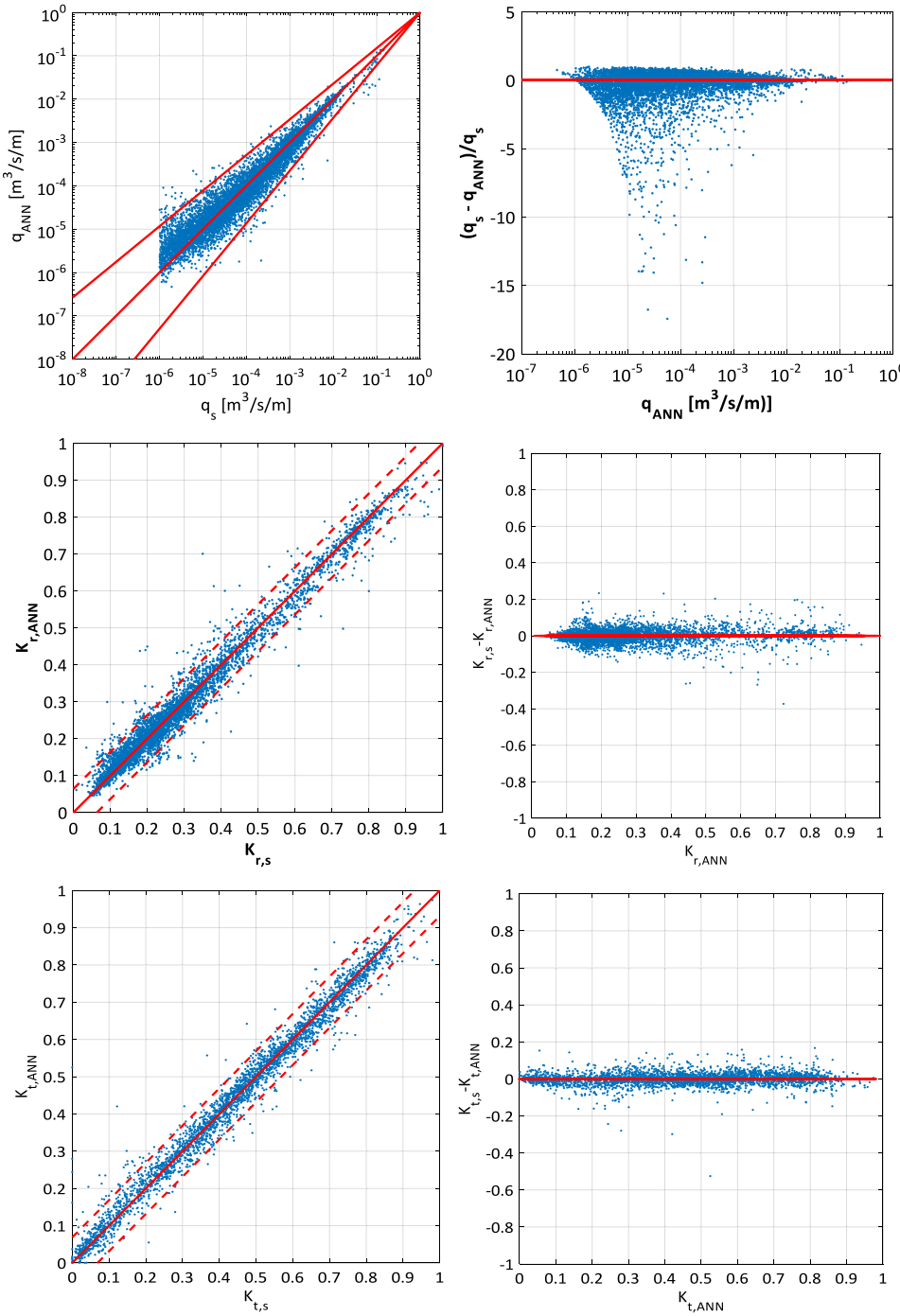

Fig. 5. From top to bottom: performance for q, K_r and K_t. To the left: comparison between predicted values (denoted by the "ANN" subscript) and corresponding measurements (denoted by the "s" subscript); to the right: difference between predictions and measurements as a function of the predictions.

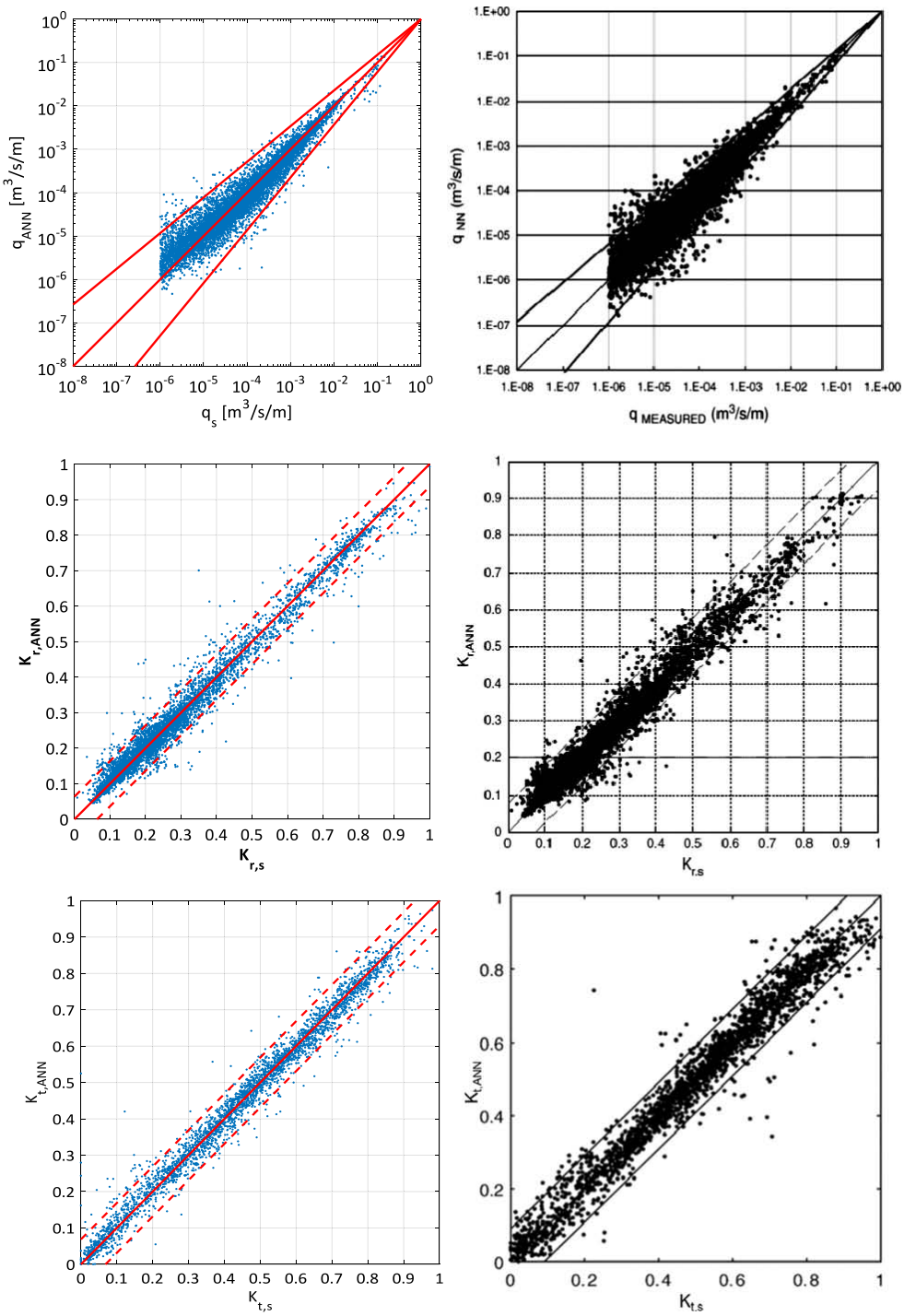

Fig. 6. From top to bottom: predicted values (denoted by the "ANN" subscript) against corresponding measurements (denoted by the "s" subscript) of q, K_r and K_t. To the left: performance of the new ANN tool; to the right: performance of the existing ANNs, plots derived from Van Gent *et al.* [2007], Zanuttigh *et al.* [2013] and Panizzo and Briganti [2007].

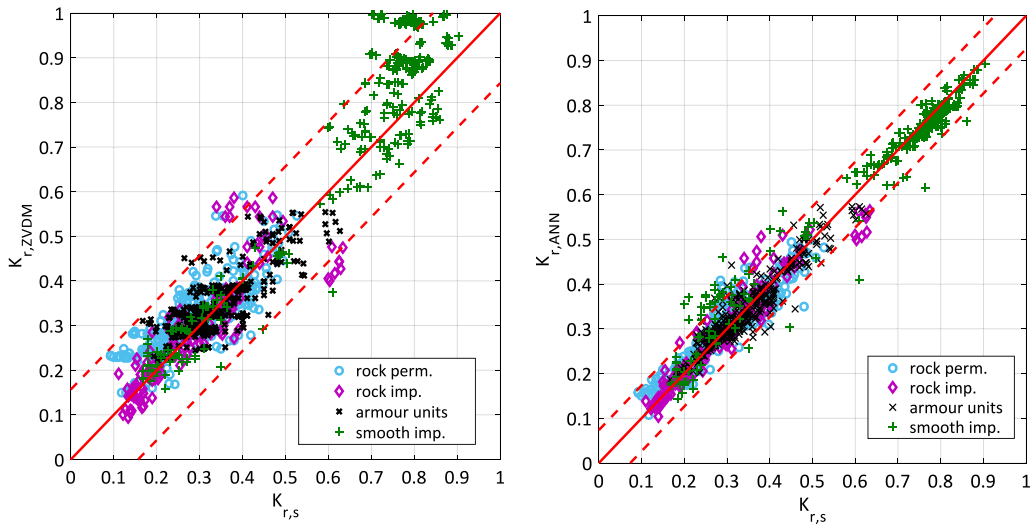

Fig. 7. Predictions obtained by the "ZVDM" formula $K_{r,\mathrm{ZVDM}}$ [Zanuttigh and van der Meer, 2006, 2008], left panel, and predictions by the new ANN $K_{r,\mathrm{ANN}}$ tool, right panel, versus the experimental values $K_{r,s}$. The different armor units are highlighted in the figures by means of different colors.

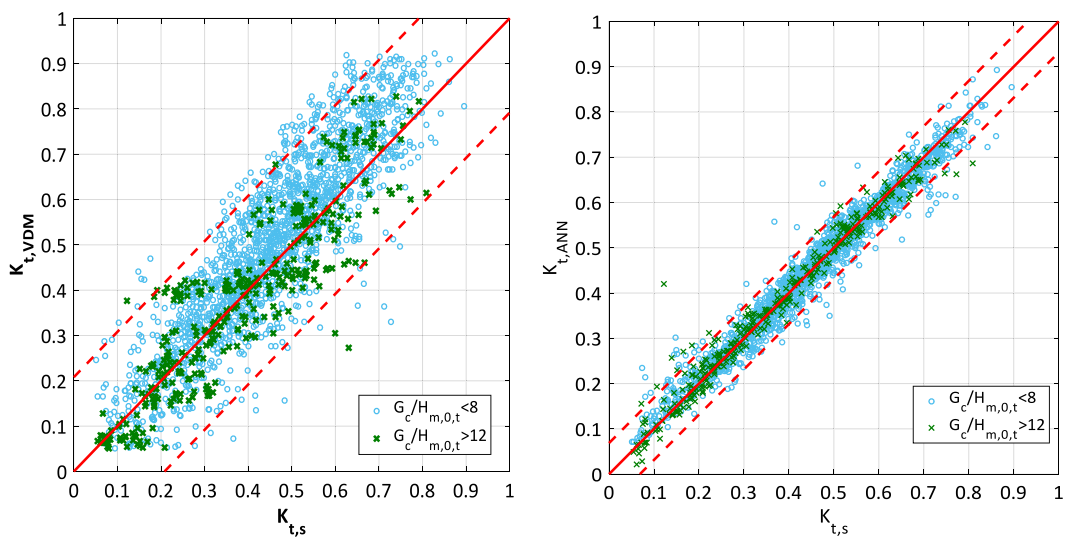

Fig. 8. Predictions obtained by the "VDM" formula $K_{t,\mathrm{VDM}}$ [Van der Meer *et al.*, 2005], left panel, and predictions by the new ANN $K_{t,\mathrm{ANN}}$ tool, right panel, versus the experimental values $K_{t,s}$. The tests belonging to the different classes of $G_c/H_{m0,t}$ are highlighted in the figures by means of different colors.

The results of the sensitivity analysis are shown in Fig. 4 after 500 *bootstrap* resampling in terms of the average Root Mean Square Error (RMSE) values and the related standard deviations. In case of q, the index RMSE* computed from the transformed values of q (see Sec. 3.6) is used.

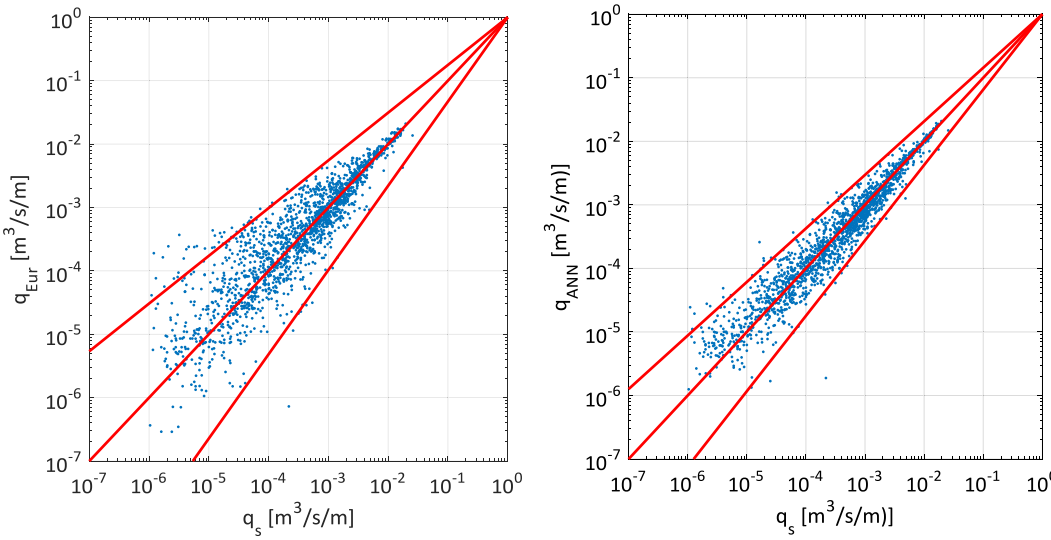

Fig. 9. Predictions obtained by the EurOtop [2016] formulae, qEur, left panel, and predictions by the new ANN tool, $q_{,\mathrm{ANN}}$, right panel, versus the experimental values q_s.

The combined analysis of the average RMSE and of the standard deviation was not considered by previous works. Figure 4 shows that the minimum of the standard deviations is achieved for $N_{\mathrm{hn}} = 20$ and that the uncertainty associated to the predictions tends to increase by further increasing the size of the hidden layer. This phenomenon is a direct consequence of the over-fitting that occurs when the ANN architecture reaches a considerable level of complexity (i.e. too high number of connections among parameters and neurons, and therefore of N_{fd}).

These considerations and the trend of the average values of the ANN error suggest to select 20 hidden neurons for both K_r and K_t. As for q, the average error decreases from 20 to 30 hidden neurons, while the standard deviation increases. In order to avoid risks of over-fitting and assure a greater capability of generalization (i.e. predicting "new data"), the final number of 20 hidden neurons was selected also for q. This choice allows also to keep the same ANN architecture for the three outputs.

3.6. *Assessment of the neural network performance*

For the quantitative assessment of the accuracy of the ANN predictions, the following three error indexes are employed: the RMSE, the Willmott index, WI [Wilmott, 1981] and the coefficient of determination, R^2, respectively defined as

$$\mathrm{RMSE} = \sqrt{\frac{1}{N}\sum_{j=1}^{N}(y_{s,j} - y_{\mathrm{ANN},j})^2}, \tag{8}$$

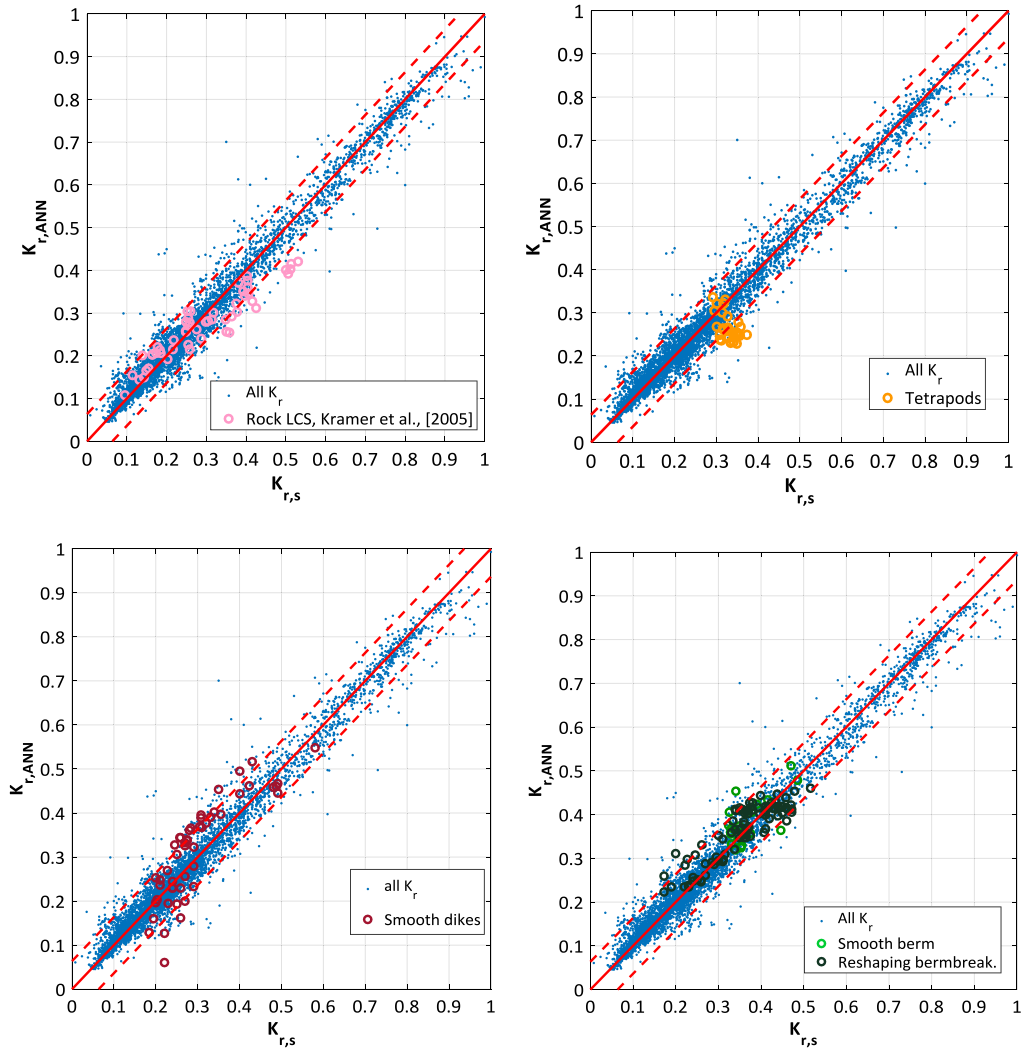

Fig. 10. Comparisons among the ANN predictions and corresponding measurements of K_r. The predictions of the new datasets are highlighted with different colors and compared to the overall ANN predictions (sky blue).

$$\mathrm{WI} = 1\frac{\sum_{j=1}^{N}(y_{s,j} - y_{\mathrm{ANN},j})^2}{\sum_{j=1}^{N}[|y_{s,j} - \langle y_s\rangle| + |y_{\mathrm{ANN},j} - \langle y_s\rangle|]^2}, \tag{9}$$

$$R^2 = 1 - \frac{\sum_{j=1}^{N}(y_{s,j} - y_{\mathrm{ANN},j})^2}{\sum_{j=1}^{N}(y_{s,j} - \langle y_s\rangle)^2} \tag{10}$$

where the quantity "y" is the output parameter, given by $q*$ [see the definition below, Eqs. (11) and (12)] or K_r or K_t; the subscripts "s" and "ANN" denote the experimental and the predicted quantity respectively, and the mean experimental

value appearing in Eqs. (9) and (10) is $\langle y_s \rangle = \frac{1}{N} \sum_{j=1}^{N} y_{s,j}$, where N is the number of tests and the subscript j indicates the jth test of the database.

These different indexes defined in Eqs. (8)–(10) are introduced to examine different aspects of the ANN performance.

The RMSE, Eq. (8), shows the dispersion of the predicted values with respect to the measured ones, therefore the lower the RMSE, the more accurate the prediction. Its numerical value depends on the order of magnitude of the associated output parameter, and therefore it has different ranges for K_r and K_t with respect to q. To allow a direct comparison of the performance of the ANN tool in terms of RMSE among the three application cases, the values of q used for training are preliminary rescaled to fit the same range $[0, 1]$ as K_r and K_t. Specifically, the training values of q in the database are scaled as follows

$$q^* = \frac{\log_{10}(q_{\mathrm{AD}}) - \min\{\log_{10}(q_{\mathrm{AD}})\}}{|\min\{\log_{10}(q_{\mathrm{AD}})\} - \max\{\log_{10}(q_{\mathrm{AD}})\}|}. \tag{11}$$

The target output for the ANN becomes the quantity q^*, computed as in Eq. (11), where the experimental values appear in the dimensionless form q_{AD} [adopted also by Van Gent *et al.*, 2007]

$$q_{\mathrm{AD}} = \frac{q}{\sqrt{g H_{m,0,t}^3}}. \tag{12}$$

For clarity, the RMSE computed from the transformed values q^* will be hereinafter denoted accordingly with the symbol

$$\mathrm{RMSE}^* = \sqrt{\frac{1}{N} \sum_{j=1}^{N} (q^*_{s,j} - {q^*}_{\mathrm{ANN},j})^2}. \tag{13}$$

The values reported in Table 4 correspond to Eq. (13), while the plots showing the ANN performance for q are instead derived by re-transforming again the predictions back to the original scale of the experimental values and in dimensional form, i.e. through the inverse functions of Eqs. (11) and (12).

WI and R^2 are normalized indexes and therefore range between 0 and 1, being 1 the perfect correspondence. R^2 accounts for the distribution of the experimental values around the mean, while WI accounts also for the distribution of the prediction with respect to the same experimental mean. WI is thus a symmetry indicator. The logarithmic transformation does not affect the normalized values of WI and R^2.

In addition to Eqs. (8)–(10), the analysis includes also the quantification of what the authors define as "large errors". They correspond to the percentage of tests, with respect to the total number of tests, for which the ANN tool gives "systematically" an output value that differs more than 1.5 times from the experimental corresponding value. Systematically here it means in more than 50% of the predictions.

As the final predictions are derived from the commitment of more ANNs created through the bootstrap resampling of the training database (see Sec. 4.1), all the performance indexes in Tables 4 and 6 are derived from averaging the values of Eqs. (8)–(11) on the 500 bootstrap resamplings, i.e.:

$$\begin{aligned} \mathrm{RMSE} &= \frac{1}{500}\sum_{i=1}^{500}\mathrm{RMSE}_I, \quad \mathrm{WI} = \frac{1}{500}\sum_{i=1}^{500}\mathrm{WI}_i, \\ R^2 &= \frac{1}{500}\sum_{i=1}^{500}R_i^2, \quad \mathrm{RMSE}^* = \frac{1}{500}\sum_{i=1}^{500}\mathrm{RMSE}_I^*, \end{aligned} \tag{14}$$

where denotes the ith performance index associated to the ith bootstrapped ANN.

4. The Results of the New ANN Tool

4.1. *Qualitative and quantitative performance*

The performance of the ANN is quantitatively given in Table 4 and is qualitatively shown in Fig. 5 for the three output parameters. The indexes in Table 4 show that the predictions of K_r and K_t are generally more accurate (see the average corresponding values of R^2), with a more symmetric error distribution (see WI) than the prediction of q. The accuracy related to the predictions of K_r and K_t is comparable, as the slightly higher values of R^2 and WI characterizing K_t are balanced by the lower standard deviations and fewer large errors associated to K_r. These results lead to the conclusion that the ANN prediction for K_t is more precise on an average, but is indeed affected by a larger dispersion of the error than the ANN prediction for K_r.

Figure 5 shows a fair agreement of computations and measurements for all the three output parameters. To the left of Fig. 5, the values computed by the ANN are compared with the measured values. The bisector line represents the perfect correspondence among predicted and experimental values; therefore, the dispersion of the points qualitatively indicates the performance of the ANN with respect to the optimal prediction. To the right, the difference among predictions and measurements is shown as a function of the predictions.

The scatter associated to K_t is extremely limited. The most evident deviations are associated to the lowest measurements, i.e. $K_{t,s} < 0.05$ (see Fig. 5 to the left). For K_r, a greater dispersion is detected. The largest errors correspond to structures characterized by nonstraight slopes and composite geometries, which are groups E and F of the database, see Sec. 2. Nevertheless, the difference among measurements and predictions is almost "always" in the range $[-0.2; 0.2]$.

With the exception of the prediction of q, the ANN results are characterized by a good degree of symmetry and no evident bias against the predicted values is observed (see Fig. 5 to the right). The ANN tends to systematically overestimate the low values of q_s and overall the distribution of the relative error $(q_s - q_{\mathrm{ANN}})/q_s$

is biased with respect to the mean red line (see Fig. 5, right). The highest scatter is obtained around $q_{\mathrm{ANN}} = 10^{-4}\,\mathrm{m}^3/\mathrm{s/m}$, where most of the experimental data are indeed concentrated. The lower the q_s, the more evident the asymmetry. The tendency to overestimate the lowest values of q is expected to be due to the elimination of the "small" values of q [following Van Gent *et al.*, 2007] in the training process.

It was verified that the ANN predictions do not show any relevant bias depending on the input parameters.

4.2. *Comparison with existing ANNs*

This sub-section presents the comparison among the new ANN tool and other ANNs available in the literature:

- the wave overtopping ANN developed within the CLASH framework [Van Gent *et al.*, 2007];
- the wave reflection ANN developed during the THESEUS project [Zanuttigh *et al.*, 2013];
- the wave transmission ANN developed as a follow-up of the DELOS project [Panizzo and Briganti, 2007].

The input parameters characterizing the 3 ANNs and the new ANN tool are summarized in Table 5. The number and the type of these parameters are elements of comparison with the new ANN tool, because they affect the architecture complexity and establish the number of freedom degrees to be calibrated (i.e. N_{fd}, see Sec. 3.2). The value of $N_{\mathrm{fd}} = 341$, Eq. (5), associated to the new ANN tool is significantly lower in comparison to the 601 characterizing the wave reflection ANN and is exactly the same as the overtopping ANN. The significant increase of N_{fd} with respect to the transmission ANN (characterized by $N_{\mathrm{fd}} = 55$) is justified by the goal to represent all the three outputs with the same ANN and it is indeed not an issue given the size of the training database for K_t, that now collects 3275 (i.e. nearly 10 times the value of N_{fd}).

The quantitative results of the performance of the three existing ANNs, reported in Table 6, allow only a partial comparison with the new ANN tool, because many error indexes are not available from previous works. Anyway, by comparing the results in Table 6 with the ones in Table 4, it can be observed that the new ANN tool provides sensibly more accurate predictions of K_r and K_t than the corresponding existing ANNs, especially in terms of R^2 (available for both K_r and K_t) and WI (only for K_r). The improvement associated to K_t can be easily explained by the substantial increase in the number of input parameters (comparing Tables 3 and 5), while the better behavior in the case of K_r may be justified by the revised selection of the input parameters, the adoption of the bootstrapping and the "commitment of networks" (see Sec. 3.4) and the extension of the training database.

Due to the different ways of defining the target values for q, (see Sec. 3.6), the additional index RMSE has been derived to characterize the performance of the new ANN tool according to the same definition used by Van Gent *et al.* [2007] that was based on $\log(q_{\mathrm{AD}})$ instead of q^*. The resulting value of RMSE $= 0.293$ is exactly the same as the RMSE $= 0.29$ associated to the CLASH ANN (see Table 6).

The qualitative comparison among the predictions obtained with the existing ANNs (right) and with the new ANN tool (left) is given in Fig. 6. The graphs of Fig. 6-left are the same of Fig. 5-left and are reproduced to make the comparison easier for the reader. The new ANN tool considers more data than the existing ANNs, both in training and in prediction.

In agreement with the quantitative results of Table 6, the new ANN tool gives narrower confidence bands and reduced scatter for both K_r and K_t, where the most remarkable improvement is undoubtedly associated to K_t. Both the new ANN tool and the existing ANN overestimate the low values $q_s < 10^{-4}\,\mathrm{m^3/s/m}$. However, the new ANN is characterized by wider confidence intervals and more pronounced bias, compared to the CLASH ANN. Further research significantly improved the prediction of q by the new ANN tool through the extension of the training database to all the $q > 0$ values, see Zanuttigh *et al.* [2016], and EurOtop [2016].

4.3. *Comparison with existing formulae*

The present sub-section provides a comparison of the performance of the new ANN tool against some of the most recent traditional formulae for the prediction of K_r, K_t and q.

- The formula by Zanuttigh and van der Meer [2006, 2008] was selected for the prediction of K_r:

$$K_r = \tanh(a \cdot \xi_{m-1,0}^{b}),$$
$$\text{where } \begin{cases} a = 0.167 \cdot [1 - \exp(-3.2 \cdot \gamma_f)] \\ b = 1.49 \cdot (\gamma_f - 0.38)^2 + 0.86 \end{cases} \text{ and } \xi_{m-1,0} = \frac{\tan\alpha}{\sqrt{\frac{2\pi H_{m,0,t}}{g T_{m-1,0}^2}}}. \quad (15)$$

  Equation (15) is valid in "design conditions" (i.e. $R_c/H_{m,0,t} \geq 0.5$, $H_{m,0,t}/D \geq 1.0$, $H_{m,0,t}/L_{m-1,0,t} \geq 0.01$) and in case of straight slopes under perpendicular wave attack, therefore 1219 tests within the database were accordingly considered for prediction: 337 tests belonging to the group A, 117 to group B, 416 to group C and 349 to group D.
- The formulae by Van der Meer *et al.* [2005] were considered for the prediction of K_t behind low-crested structures:

$$K_t = -0.4\frac{R_c}{H_{m0,t}} + 0.64\left(\frac{G_c}{H_{m0,t}}\right)^{-0.31}(1 - e^{-0.5\xi_{0,p}}), \quad \text{if } \frac{G_c}{H_{m0,t}} < 10, \quad (16)$$

$$K_t = -0.35\frac{R_c}{H_{m0,t}} + 0.51\left(\frac{G_c}{H_{m0,t}}\right)^{-0.65}(1 - e^{-0.41\xi_{0,p}}), \quad \text{if } \frac{G_c}{H_{m0,t}} > 10, \quad (17)$$

where $\xi_{0,p} = \frac{\tan\alpha}{\sqrt{\frac{H_{m0,t}}{L_{0,p}}}}$ and L_{0p} is the offshore wave length associated to the peak wave period T_p. Equations (16) and (17) are limited by $K_t \geq 0.05$ and by the condition $K_t = -0.006 \cdot G_c/H_{m,0,t} + 0.93$. Van der Meer *et al.* [2005] suggested to use Eq. (16) for $G_c/H_{m0,t} < 8$ and Eq. (17) for $G_c/H_{m0,t} > 12$ and to interpolate in the range $8 < G_c/H_{m0,t} < 12$. Equations (16) and (17) and the new ANN tool were applied on two datasets composed by 2128 ($G_c/H_{m0,t} < 8$) and 530 ($G_c/H_{m0,t} > 12$) tests, respectively.

- The formulae from the EurOtop [2016] manual were selected for the prediction of q:

$$\frac{q}{\sqrt{g \cdot H_{m0,t}}} = \frac{0.023}{\sqrt{\tan\alpha}} \cdot \gamma_b \cdot \xi_{m-1,0} \cdot \exp\left(-\left(2.7 \cdot \frac{R_c}{\xi_{m-1,0} \cdot H_{m0,t} \cdot \gamma_b \cdot \gamma_f \cdot \gamma_\beta \cdot \gamma_v}\right)^{1.3}\right), \quad \text{for non-breaking waves,} \quad (18)$$

with a maximum of

$$\frac{q}{\sqrt{g \cdot H_{m0,t}}} = 0.09 \cdot \exp\left(-\left(1.5 \cdot \frac{R_c}{\xi_{m-1,0} \cdot H_{m0,t} \cdot \gamma_f \cdot \gamma_\beta}\right)^{1.3}\right), \quad \text{for breaking waves.} \quad (19)$$

These formulae are valid for sloping structures with zero and positive freeboard ($R_c >= 0$) and for values of $\xi_{m-1,0} < 5$. Since it was not possible to precisely reconstruct the datasets used to calibrate Eqs. (18) and (19), all the tests with berms, toe protections and nonsmooth surface (i.e. $\gamma_f \neq 1$) were excluded, leading to 1'806 tests including only straight smooth impermeable slopes with experimental values of $q_s > 10^{-6}\,\mathrm{m}^3/\mathrm{s/m}$.

The quantitative comparison among the formulae in the literature and the ANN performance is provided in Table 7. For K_r and K_t, the values of the performance indexes are grouped by different datasets according to the distinctions made by the formulae. The qualitative comparison is further investigated in Figs. 7–9, for K_r, K_t and q, respectively. The bisector represents the perfect correspondence, while the external lines refer to the 95% confidence bands. In Figs. 7 and 8 the data belonging to the different class of armour units (Fig. 7) and values of $G_c/H_{m0,t}$ (Fig. 8) are highlighted with different colors, in accordance to the datasets of Table 7.

All the Figs. 7–9 show that the ANN predictions are definitely less scattered and more symmetric, and the 95% confidence bands are systematically narrower than for

the formulae. From Fig. 7-left, even if most of the predictions derived from Eq. (15) are aligned along the bisector, it is evident that some datasets (rock permeable and armor units) are better predicted than others (especially the smooth impermeable structures). Similarly, in Fig. 8-left, the tests with $G_c/H_{m0,t} > 12$ are generally less scattered and less biased than the tests with $G_c/H_{m0,t} < 8$. On the contrary, the ANN predictions of both K_r and K_t do not show any dependence on the armor type or on the value of $G_c/H_{m0,t}$, being all the data predicted with a similar accuracy. The same conclusions can be drawn by comparing the quantitative performance indexes of Table 7.

As for q, Fig. 9 suggests that the highest values of overtopping ($q > 5 \cdot 10^{-3}\,\mathrm{m^3/s/m}$) are similarly well-predicted by both the formula [Van der Meer *et al.*, 2013] and by the ANN. On the contrary, the ANN is significantly more accurate when predicting lower values of q, as in the worst case the error is of one order of magnitude whereas some of the predictions computed by the formula may be overestimated of two orders of magnitude. Actually, Eqs. (18) and (19) are targeted to provide cautious estimates of the overtopping discharge.

Overall, the ANN is able to overcome the "limit" and the discontinuities of the conventional formulae for all the output parameters, K_r, K_t and q, even if this should be explained by taking into account the significantly higher number of involved parameters (15 input parameters and overall 341 degrees of freedom).

4.4. *Test of the ANN capability of generalization*

This subsection aims to evaluate the ANN capability of generalization, i.e. of predicting data not used in training but whose parameters still fall in the range of the training database. To this purpose, some datasets belonging to the reflection database have been excluded from the training process and used exclusively in prediction. This of course required a re-training of the reflection ANN on a narrower database, leading to slightly different sets of weights and biases. Overall, 261 tests belonging to the following 5 datasets have been removed from the training:

- 53 tests on rock LCS [Kramer *et al.*, 2005]: in this case the whole dataset of Wave Flume tests carried out at Catalunya University was removed; section "A");
- 50 tests on tetrapods breakwater (confidential source; section "C");
- 43 tests on smooth dikes (confidential source; section "D");
- 20 tests on smooth berms (confidential source; section "E");
- 95 tests of 3D wave attacks on reshaping berm-breakwaters (confidential source; section "E").

The choice of these data (both as number and type) was done to verify the ANN performance against different kinds of structure and to contemporarily preserve the variety and size of the training database in order to get an ANN that does not differ significantly from the original one. The two differently trained ANNs are indeed

characterized by the same performance, as it can be appreciated by comparing the values of the corresponding error indexes, reported in the first row of Tables 8 and 4, respectively.

The quantitative results of the prediction of the "new" datasets are collected in Table 8 (rows 2–7), while the comparison among measured and predicted values of K_r is provided in Fig. 10. In the diagrams of Fig. 10, the new predicted data are highlighted with different colors and compared to the predictions of the complete database derived from the optimized ANN.

On an average, approximately 70% of the predictions fall within the 95% confidence bands and no significant bias is observed. A few outliers are present in all the datasets. Generally, the scatter is limited and not greater than the one associated to the prediction of the complete database, being the greatest errors approximately of the 30–35% (e.g. $K_{r,\mathrm{ANN}} \approx 0.35$ instead of $K_{r,s} \approx 0.5$ in the case of the smooth berms, and $K_{r,\mathrm{ANN}} \approx 0.25$ instead of $K_{r,s} \approx 0.38$ for the tetrapods, see Fig. 10).

The values of the indexes in Table 8 are comparable to the overall performance of the optimized ANN (see Table 4), especially considering RMSE and WI. However, the R^2 are sensibly lower and the standard deviations higher of at least one order of magnitude. The best-represented datasets are the reshaping berm-breakwaters (only 3% of the predictions exceeds the confidence bands). The worst performance is achieved for the tetrapods, with roughly 50% of data out of the confidence bands, and with values of the standard deviations of the same order of magnitude of the average values of R^2 and WI.

The ANN capability of predicting the reshaping berm-breakwater dataset is particularly meaningful, because such dataset represents a very special combination of wave conditions and structure cross-section. The range of variability of $h_b/H_{m0,t} = -2.12 - -0.54$ describes, on one hand, the presence of a very emerged berm; and on the other hand, the value of -2.12 corresponds to the absolute lower limit of $h_b/H_{m0,t}$ within the training range of the reflection ANN (see Table 2). The reshaping profiles certainly induce additional uncertainty into the determination of the actual reflection process, due to the slope changes during the test. More reshaping gives larger scatter. It is worthy to mention that reshaping berm breakwaters are included in the database with the initial profile. The ANN performance is rather good, revealing a satisfactory capability of dealing with complex and nonstandard cross-sections also.

5. Conclusions

This paper presents an optimized ANN tool able to accurately predict the overtopping discharge q, the wave transmission coefficient K_t and the wave reflection coefficient K_r for a wide range of structure geometries and wave conditions. The final tool consists of three similar ANNs, trained on three specific datasets of q, K_r and K_t, and providing separately each output parameter.

This tool with the database will be released to the engineering community at the following link: www.unibo.it/overtopping-neuralnetwork. The tool is also part of the update of EurOtop manual [2016, in press].

The ANN was trained on the new extended database, based on CLASH [2004], and consisting now of nearly 18,000 tests. The database was prepared following the same structural and hydraulic schematization as in CLASH and including the following additional information: K_t and K_r, where available; the average unit size D, representative of the structure elements and the characteristic downslope D_d and upslope D_u sizes of the elements in the run-up/down area; the roughness factors γ_{fd} and γ_{fu} of the downslope and the upslope; a new label to identify possible special features of the tests and selecting the data to be used for the ANN training.

The 15 selected input parameters of the ANN are all made dimensionless with the significant wave-height or spectral wave length to represent specific physical processes, such as shoaling, breaking and reflection from the structure.

The optimal architecture of the new ANN tool was setup by means of a careful sensitivity analysis to the key elements of the training and the learning processes, which are the training algorithm, the number of hidden neurons and the early-stopping technique. The employment of the *bootstrap* resampling technique improves the capability of generalization of the ANN, i.e. the capability to predict new data, and allows to derive the predictions associated to statistical quantiles, i.e. to assess its performance.

The ANN predictions of the data used for training give RMSE values in the range of 0.03–0.05. The analysis of the error distribution shows that the ANN behavior is not biased depending on a specific dataset or input parameter.

The ANN accuracy is much greater than recent existing formulae [Van der Meer *et al.*, 2005, 2013; Zanuttigh and van der Meer, 2008], even considering only data falling in the range of applicability of the formulae themselves. This result may be expected as the ANN is characterized by more parameters and is trained to deal with more complex structures and a wider range of wave conditions than the formulae.

This new ANN tool is also more accurate than the specific ANNs developed for K_t [Panizzo and Briganti, 2007] and for K_r [Zanuttigh *et al.*, 2013] on narrower datasets. Moreover, it is as accurate as the CLASH ANN [Van Gent *et al.*, 2007] for predicting q, being characterized by the same RMSE.

The ANN robustness is proved by the fair predictions of K_r for new datasets. Yet, it is strongly recommended to check the range of each input parameter, in order to prevent the use of the ANN tool out of its training fields.

Acknowledgments

The first author gratefully acknowledges the support of her Research Fellowship by the European Commission through FP7.2009-1, Contract 244104 — THESEUS project ("Innovative technologies for safer European coasts in a changing climate"),

www.theseusproject.eu. The collaboration between the University of Bologna and Van der Meer is voluntary work from the second and the third authors.

References

Besley, P., Reeves, M. & Allsop, N. W. H. [1993] "Random wave physical model tests: Overtopping and reflection performance," Report IT 384, HR Wallingford.

Bruce, T., Van der Meer, J. W., Franco, L. & Pearson, J. [2006] "A comparison of overtopping performance of different rubble mound breakwater armour," in *Proc. XXX Int. Conf. Coastal Eng.* Vol. 5, pp. 4567–4579.

CLASH [2004] "Crest level assessment of coastal structures by full scale monitoring, neural network prediction and hazard analysis on permissible wave overtopping," EC-contract EVK3-CT-2001-00058, www.clash-eu.org.

EurOtop [2016] Manual on Wave Overtopping of Sea Defences and Related Structures. An Overtopping Manual Largely based on European Research, but for Worldwide Application, Allsop, N. W. H., Bruce, T., DeRouck, J., Kortenhaus, A., Pullen, T., Schüttrumpf, H., Troch, P., van der Meer, J. W. & Zanuttigh, B., www.overtopping-manual.com.

Formentin, S. M. & Zanuttigh, B. [2013] "Prediction of wave transmission through a new artificial neural network developed for wave reflection," *Proc. 7th Int. Conf. Coastal Dynamics*, http://www.coastaldynamics2013.fr/pdf_files/057_Formentin_SaraMizar.pdf.

Goda, Y., Kishira, Y. & Kamiyama, Y. [1975] "Laboratory investigation on the overtopping rate of seawalls by irregular waves," Report of Port and Harbour Research Institute, Vol. 14, No. 4.

Hagan, M. T. & Menhaj, M. [1994] "Training feed-forward networks with the Marquardt algorithm," *IEEE Trans. Neural Netw.* **5**(6), 989–993.

Kramer, M., Zanuttigh, B., van der Meer J. W., Vidal, C. & Gironella, X. [2005] "2D and 3D experiments on low-crested structures," *Coastal Eng.* **52**, 867–888.

Liu, P. L.-F. & Lin, P. [1997] "A numerical model for breaking waves: the volume of fluid method," Research Report No. CACR-97-02, Center for Applied Coastal Research, Ocean Engineering Laboratory, University of Delaware, Newark, DE.

Losada, I. J., Lara, J. L., Guanche, R. & Gonzalez-Ondina, J. M. [2008] "Numerical analysis of wave overtopping of rubble mound breakwaters," *Coastal Eng.* **55**(1), 47–62.

Lykke Andersen, T., Skals, K. T. & Burcharth, H. F. [2008] "Comparison of homogenous and multilayered berm breakwaters with respect to overtopping and front slope stability," in *ASCE*, *Proc. ICCE 2008*, Vol. 4, pp. 3298–3309

Marquardt, D. [1963] "An algorithm for least-squares estimation of nonlinear parameters," *SIAM J. Appl. Math.* **11**(2), 431–441, doi: 10.1137/0111030.

Panizzo, A. & Briganti, R. [2007] "Analysis of wave transmission behind low crested breakwaters using neural networks," *Coastal Eng.* **54**, 643–656.

Van der Meer, J. W., Briganti, R., Zanuttigh, B. & Wang, B. [2005] "Wave transmission and reflection at low crested structures: Design formulae, oblique wave attack and spectral change," *Coastal Eng.* **52**(10–11), 915–929.

Van der Meer, J. W., Verhaeghe, H. & Steendam, G. J. [2009] "The new wave overtopping database for coastal structures," *Coastal Eng.* **56**, 108–120.

Van der Meer, J. W., Bruce, T., Allsop, W., Franco, L., Kortenhaus, A., Pullen, T. & Schüttrumpf, H. [2013] "EurOtop revisited. Part 1: Sloping structures," *Proc. ICE*, *Coasts*, *Marine Structures and Breakwaters*, Edinburgh, UK.

Van Doorslaer, K., De Rouck, J., Audenaert, S. & Duquet, V. [2015] "Crest modifications to reduce wave overtopping of non-breaking waves over a smooth dike slope," *Coastal Eng.* **101**, 69–88, doi: 10.1016/j.coastaleng.2015.02.004.

Van Gent, M. R. A., van den Boogaard, H. F. P., Pozueta, B. & Medina, J. R. [2007] "Neural network modelling of wave overtopping at coastal structures," *Coastal Eng.* **54**, 586–593.

Van Oosten, R. P. & Peixò Marco, J. [2005] *Wave Transmission at Various Types of Low-Crested Structures Using Neural Networks*, M.Sc. Thesis, TU Delft, Faculty of Civil Engineering and Geosciences, Hydraulic Engineering.

Verhaeghe, H. [2005] *Neural Network Prediction of Wave Overtopping at Coastal Structures*, Ph.D. Thesis, Universiteit Gent, Gent, BE, http://vliz.be/en/imis?module=ref&refid=75351.

Verhaeghe, H., De Rouck, J. & Van der Meer, J. W. [2008] "Combined classifier–quantifier model: A 2-phases neural model for prediction of wave overtopping at coastal structures," *Coastal Eng.* **55**, 357–374.

Victor, L. & Troch, P. [2012] "Wave overtopping at smooth impermeable steep slopes with low crest freeboards," *J. Waterway Port Coastal Ocean Eng.*, 372–385, 10.1061/(ASCE)WW.1943-5460.0000141.

Wilmott, C. J. [1981] "On the validation of models," *Phys. Geography* **2**, 184–194.

Zanuttigh, B. & van der Meer, J. W. [2006] "Wave reflection from coastal structures," *Proc. Coastal Eng. 2006*, Vol. 5, Smith, J. M. (ed.), San Diego, USA, September 3–8 2006 (World Scientific Publishing Co.), pp. 4337–4349.

Zanuttigh, B. & van der Meer, J. W. [2008] "Wave reflection from coastal structures in design conditions," *Coastal Eng.* **55**(10), 771–779.

Zanuttigh, B., Formentin, S. M. & Briganti, R. [2013] "A neural network for the prediction of wave reflection from coastal and harbor structures," *Coastal Eng.* **80**, 49–67.

Zanuttigh, B., Formentin, S. & Van der Meer, J. [2014] "Advances in modelling wave-structure interaction through artificial neural networks," *Coastal Eng. Proc.* **1**(34), 69, doi: http://dx.doi.org/10.9753/icce.v34.structures.69.

Zanuttigh, B., Formentin, S. M. & Van der Meer, J. W. [2016] "Prediction of extreme and tolerable wave overtopping discharges through an advanced neural network," *Ocean Eng.* **127**, 7–22.